Dalton Transactions

Accepted Manuscript

This is an *Accepted Manuscript*, which has been through the Royal Society of Chemistry peer review process and has been accepted for publication.

Accepted Manuscripts are published online shortly after acceptance, before technical editing, formatting and proof reading. Using this free service, authors can make their results available to the community, in citable form, before we publish the edited article. We will replace this *Accepted Manuscript* with the edited and formatted *Advance Article* as soon as it is available.

You can find more information about *Accepted Manuscripts* in the Information for Authors.

Please note that technical editing may introduce minor changes to the text and/or graphics, which may alter content. The journal's standard Terms & Conditions and the Ethical guidelines still apply. In no event shall the Royal Society of Chemistry be held responsible for any errors or omissions in this *Accepted Manuscript* or any consequences arising from the use of any information it contains.

ROYAL SOCIETY OF CHEMISTRY

www.rsc.org/dalton

Journal Name Dalton Transactions Dynamic Article Links ►

Cite this: DOI: 10.1039/c0xx00000x

www.rsc.org/xxxxxx

ARTICLE TYPE

Red Electroluminescence of Ruthenium Sensitizer Functionalized by sulfonylate Anchoring Groups

Hashem Shahroosvand[a]*, Parisa Abbasi [a], Ezeddin Mohajerani[b], Mohammad Janghouri [b]

[a]Chemistry Department, University of Zanjan, Zanjan, Iran.
[b]Laser and Plasma Research Institute, Shahid Beheshti University, Tehran, Iran.

Received (in XXX, XXX) Xth XXXXXXXXX 20XX, Accepted Xth XXXXXXXXX 20XX
DOI: 10.1039/b000000x

We have synthesized five novel Ru(II) phenanthroline complexes with additional aryl sulfonylated ligating substituent at the 5-position $[Ru(L)(bpy)_2](BF_4)_2$ (1) , $[Ru(L)(bpy)(SCN)_2]$ (2) , $[Ru(L)_3](BF_4)_2$ (3), $[Ru(L)_2(bpy)](BF_4)_2$ (4) and $[Ru(L)(BPhen)(SCN)_2]$(5) (where L= 6-one-[1,10]phenanthroline-5-ylamino)-3-hydoxy naphthalene 1-sulfonic, bpy= 2, 2′-bipyridine, BPhen= 4, 7 diphenyl, 1, 10-phenanthroline), as both photosensitizers for oxide semiconductor solar cells (DSSCs) and light emission diodes(LEDs). The absorption and emission maxima of these complexes red shifted with extending the conjugation of the phenanthroline ligand. Ru phenathroline complexes exhibit the broad metal to ligand charge transfer-centered electroluminescence (EL) with maximum near 580 nm. Our results indicated that special structure (2) can be considered as both DSSC and OLED devices. The efficiency of the LED performance can be tuned by using a range of ligands. The device (2) has a luminance of 550 cd/m^2 and maximum efficiency of 0.9 cd/A at 18 V which are the highest values among the five devices. The turn-on voltage of this device is approximately 5 V. The role of auxiliary ligands in the photopysical properties of Ru complexes was investigated by DFT calculation. We have also studied photovoltaic properties of dye-sensitized nanocrystalline semiconductor solar cells based on Ru phenanthroline complexes and an iodine redox electrolyte. A solar energy to electricity conversion efficiency (η) of 0.67 % was obtained for Ru complex (2) under the standard AM 1.5 irradiation with a short-circuit photocurrent density (J_{sc}) of 2.46 mA cm^{-2} , an open-circuit photovoltage (V_{oc}) of 0.6 V, and a fill factor (ff) of 40% which are all among the highest values in ruthenium sulfonated anchoring group reported so far. Monochromatic incident photon to current conversion efficiency was 23% at 475 nm. Photovoltaic studies clearly indicated dyes with two SCN substituent yielded a higher J_{sc} for the cell than dye with tris-homoleptic anchor substituent.

1. Introduction:

A global challenge is to capture and utilize solar energy for a sustainable development and to use the produced energy for low-cost, low-consumption lighting solutions. In this respect dye-sensitized solar cells (DSSCs) [1-6] and organic light-emitting diodes (OLEDs) [7-10] represent valuable examples of both technologies, which can also be integrated into a unique photonic device. In light harvesting, the first step in such conversion, the choice of a photosensitizer capable of efficient visible-light absorption is crucial. Therefore, many efforts have focused on the design and synthesis of various dyes, including metal complexes and organic dyes [11]. Understanding the relation between the solar cell performance and the properties of sensitizer molecule structures is one of the most important tasks for developing a high performance solar cell. Ruthenium polypyridine dyes have received much attention due to their outstanding performance as sensitizers in DSSC, reaching efficiencies of up to 11% [12-15]. At this respect, the nature of anchoring group is of outmost importance because it greatly influences the transport and adsorption of the dye into the semiconductor surface. Moreover, the knowledge of the nature and number of the binding modes and of the binding geometry is crucial factor for the study of interfacial injection processes, to improve the electrochemical devices, and to design new sensitizers. A number of Ru-polypyridine sensitizers with different anchoring moieties have been reported. Chun-Hui Huang et al. indicated that linking attaching groups such as -RSO_3^- to hemicyanine dyes can adsorb onto the surface of TiO_2 successfully and show good charge-transfer properties [16-18]. Although the formation of an ester-like linkage between carboxylic acid groups of the corresponding bipyridine ligands and TiO_2 nanocrystallites is now well established [19-22], there is a lack of experimental data on the kind of chemisorption of dyes bearing sulfonic acid functional groups. Areas of particularly strong interest have been the generation and evaluation of new dyes for intensely luminescence complexes in OLEDs. Since the discovery that $Ru(bpy)_3^{2+}$ is electroluminescence, [23, 24] a large body of literature has appeared aimed at understanding both the ground and excited state properties of $Ru(bpy)_3^{2+}$ and their derivatives [25, 26]. With the priority in electrochemical, photochemical and thermal stability, ruthenium (Ru)-based charge transfer complexes are receiving considerable attention as an important material class for light emitting device study [27, 28]. By attaching groups such as phosphonato, sulfonato or carboxylato to the bipyridine or phenanthroline moieties, Ru complexes can be linked to biological molecules such as antibodies and DNA where it serves as a tag or label for analyses, much like radioactive or fluorescent

Dalton Transactions Accepted Manuscript

labels [29]. This has resulted in a wide range of analytical applications for EL in which Ru polypyridine with anchoring group plays a key role. Moreover, the demonstration of simultaneous multi-color luminescence from metal complexes assemblies using two different strategies; the detection of a picosecond-scale luminescence component from ruthenium polypyridine complexes arising from a non-thermalised excited state; and generation of long lived charge-separated states of up to 1 second in a donor-chromophore acceptor triad. High-brightness and high-efficiency emissions with low-driving voltage of Ru-complex-based solid and solution-state EL cells have been achieved [30, 31]. Finally, Ru polypyridine complexes with anchoring group exhibit a variety of low-lying electronically excited states (p–p*, d –d*, d–p* and MLCT) which will be good candidate for both dye sensitized solar cells and light emission diodes. This paper concerns the synthesis of five novel ruthenium polypyridine complexes by using Π-extended phenanthroline ligand. Our efforts are focused on the finding a dye which could be used as both dye sensitizes solar cell and light emission diodes.

2. Experimental:

2.1 Material and Instruments. All chemicals and solvents were purchased from Merck & Aldrich and used without further purification. IR spectra were recorded on a Perkin-Elmer 597 spectrometer. ^{1}H-NMR spectra were recorded by use of a Bruker 250 MHz. Electrochemical measurements were made in DMF using model 273 A potentiostat. Electrochemical experiments were carried out in an airtight single-compartment cell by using platinum working and counter electrodes and a silver spiral as a quasi-reference electrode. The supporting electrolyte was 0.1 M $[Bu_4N]BF_4$. Ferrocene was added as an internal standard after each set of measurements, and all potentials reported were quoted with reference to the ferrocene-ferrocenium (Fc/Fc^+) couple at a scan rate of 100 mV/s. The oxidation (E_{ox}) and reduction (E_{red}) potentials were used to determine the HOMO and LUMO energy levels using the equations E_{HOMO} =- (E_{ox} + 4.8) eV and E_{LUMO} = -(E_{red} + 4.8) eV which were calculated using the internal standard ferrocene value of -4.8 eV with respect to the vacuum [32, 33]. The PL spectra of the ruthenium compounds and PVK: PBD were measured in 1,2-dimethylformamide solution. The PL spectra were recorded by ocean optic spectrometer USB2000 during 405 nm irradiation. The photocurrent-voltage (I-V) characteristics were recorded using a computer-controlled Keithley 2400 source meter under air mass(AM) 1.5 simulated illumination (100 $mWcm^{-2}$). The action spectra of monochromatic incident photo-to-current conversion efficiency (IPCE) for solar cells were performed using a commercial setup for IPCE measurement (PV-25 DYE, JASCO). Full geometric optimization and the calculation of the energetics for all of the structural variables were obtained using the B3LYP//LanL2DZ method. All calculations and optimizations were performed using the Gaussian 03 package [34].

2.2 Preparation of EL devices and testing. The structure of the fabricated device is as follow:
ITO/PEDOT:PSS(90nm)/PVK:PBD(70nm)/Al(200nm)and,
ITO/PEDOT:PSS(90nm)/PVK:PBD: ruthenium complex (70nm)/Al(200nm), That is shown in Figure 1.
PVK as a hole-transporting and PBD as an electron-transporting material were doped with ruthenium compounds. Glass substrates, coated with ITO (sheet resistance of 70 Ω/m^2), were used as the conducting anode. The ratio of ruthenium complexes for each type were 10 % Wt in PVK: PBD(100:40). PEDOT: PSS(poly(3,4-ethylenedi-oxythiophene):poly(styrenesulfonate)) was used as a hole injection and transporting layer.

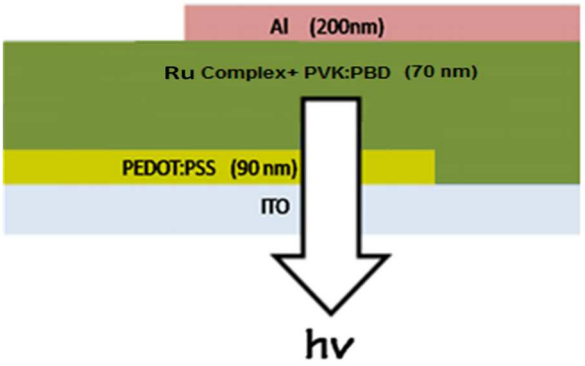

Figure 1. The layer arrangement of Ru-based LED-device .

All polymeric layers were successively deposited onto the ITO coated-glass by using spin-coating process from the solution. A metallic cathode of Al was deposited on the emissive layer at 8×10^{-5} mbar by thermal evaporation. The PEDOT: PSS was dissolved in DMF, spin coated on ITO and was held in an oven at 120 ^oC for 2 hours after deposition. PVK: PBD and ruthenium complexes with ratio of 10: 4: 1 were blended in DMF, and then spin coated and baked at 80°C for 1 hour. The thickness of the polymeric thin film was determined by a Dektak 8000. The EL intensity and spectra were measured with an ocean optic USB2000, under ambient conditions. In addition, Keithley 2400 sourcemeter was used to measure the electrical characteristics of the devices.

2.3 Fabrication of DSSC. To prepare the DSC working electrodes, the transprance conductive oxid (TCO) glass used as current collector was first cleaned in a detergent solution using an ultrasonic bath for 15 min, and then rinsed with water and ethanol. The mesoscopic TiO_2 film used as photoanodes consisted of layers of TiO_2. $TiCl_4$ treatment was applied to the prepared TiO_2 films. The sintered TiO_2 films were dipped in an aqueous solution of 50 mM $TiCl_4$ at 70 °C for 30 min, and sintered again for 30 min at 450 °C (10 µm thick transparent layer of 25 nm TiO_2 anatase nanoparticles and a 5 µm thick scattering layer of 400 nm anatase TiO_2 particles). The sintered TiO_2 electrode was then immersed for 16 h in a 3×10^{-4} M DMF solution of the dyes. The counter electrode was prepared on a bare FTO substrate. The Pt precursor was prepared by H_2PtCl_6, and spread on the front side of the FTO glass. The electrolyte consisted of 0.1 M LiI, 0.03 M I_2, and 0.5M 4-tert-buytylpyridine in 3-methoxypropionitrile.

2.4 Synthesis of ligand and complexes.

2. 4. 1 Synthesis of 6-one-[1,10] phenanthroline-5-ylamino-3-hydoxy naphthalene 1-sulfonic acid (L). The 1, 10 phenanthroline 5, 6- dione ligand was prepared according to the literature method [35]. For synthesis of (L), the 1, 10 phenanthroline 5,6- dione (100mg, 0.48mmol) and 5-ylamino-3-hydoxy naphthalene 1-sulfonic acid (0.114g, 0.48mmol) were taken in ethanol (50ml) and refluxed for 4h. After solvent evaporation at room temperature, dark red powder was appeared. This product was future purified by column chromatography using alumina as column support and chloroform/ methanol (6: 10, v/v) as the eluent. The major band was collected and corresponds to the desired ligand. Yield 82%.; m.p. =232 °C.; ^{1}H NMR (250 MHz, *DMSO, d*), (see scheme S1, ESI†) for proton labeling: δ=10.22(br.), 9.68(s, 1H, H4), 9.08(d, 2H, H3), 8.73(d, 2H, H5), 8.13(d, 2H, H1), 7.66(t, 2H, H6). CHN, Anal. Calc.: for (L),

Dalton Transactions Accepted Manuscript

This journal is © The Royal Society of Chemistry [year]

($C_{22}H_{13}N_3O_5S$): C, 61.250; H, 3.034; N, 9.740. Found: C, 61. 208; H, 2. 980; N, 9.712 % .This component will be denoted by (L).

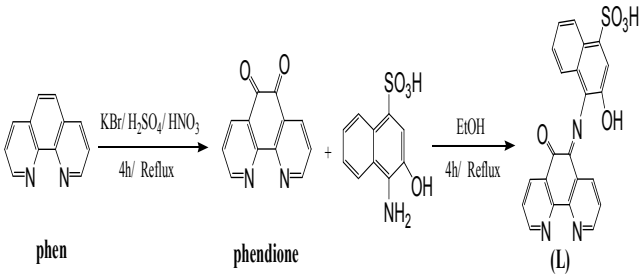

Scheme 1. Synthesis procedure of (L)

Homoleptic and hetroleptic of Ru(II) complexes were synthesized by standard procedures according to Scheme 2.

2. 4. 2. Synthesis of $[Ru^{II}(bpy)_2(L)](BF_4)_2$ *(1).* For complex (1), in a 100 ml round-bottomed flask with three vertical necks, combined with a gas-inlet, and a condenser combined with gas-outlet, under nitrogen was introduced 1 equiv. of (L) 0.07g (0.16mmol) and 1 equiv. of trichlororuthenium(III) 0.0364g (0.16 mmol). The necessary amount of degassed ethanol to solubilize the solids was added and the mixture was refluxed for 4 h. To this intermediate complex was added the 2 equiv of 2, 2-bipyridine(bpy) 0.054g (0.32 mmol) in the minimum volume of dry and degassed ethanol. Then, excess $NaBF_4$ (0.06g) was added and the solution was refluxed for a future 4 h. After this time, the reaction mixture was allowed to cool, and the precipitate was filtered and washed with deionized water, ethanol and diethyl ether. This product was future purified by column chromatography using alumina as column support and acetonitrile/ methanol (2: 1, v/v) as the eluent. The major brown band was collected and corresponds to the desired complex. . Yield 62%.; m.p. >250 °C.; ^{1}H NMR (250 MHz, *DMSO,d*), **δ**=10.35 (br.), 9.68 (s, 1H, H4), 9.06 (d, 2H, H3), 8.90 (d, 2H, H5), 8.82 (q,4H, Hd, Hd′), 8.25-8.31 (m, 6H, Ha, Ha ′, H1), 8.19(t, 4H, Hb, Hb′), 8.1-7.93 (m, 4H, Hc, Hc′), 7.85(t, 2H, H2), 7.68(t, 2H, H6).; CHN, Anal. Calc.: ($C_{42}H_{29}N_7O_5SB_2F_8Ru$) : C, 51.233; H, 6.015; N, 16.654. Found: C, 51.276; H, 6.042; N, 16.612 %

2. 4. 3. Synthesis of $[Ru^{II}(bpy)(L)(SCN)_2]$ *(2).* $[Ru^{II}(bpy)(L)(SCN)_2]$ (2**)** was prepared starting from $RuCl_3.xH_2O$ (0.036g, 0.16 mmol), bpy (0.027 g, 0.16 mmol) and L1 (0.036 g, 0.12 mmol) using the same procedure as described for Synthesis of $[Ru^{II}(bpy)_2(L)](BF_4)_2$ (1**)** except an excess of KSCN instead of $NaBF_4$ was added to the brown mixture (10 times the stoichiometric amount) and the mixture refluxed for 4 h. The reaction mixture was allowed to cool to room temperature before being filtered through a sintered glass crucible. The fine black powder in suspension was recovered by centrifugation at the speed of 5000 t/min during 15 min. Subsequently, the products were washed with water, ethanol and diethyl ether three times and dried in air at room temperature. This product was future purified by column chromatography using alumina as column support and acetonitrile/ methanol (2: 1, v/v) as the eluent. The major dark brown band was collected and corresponds to the desired complex. Yield: 52%.; m. p. >250 °C.; ^{1}H NMR (250 MHz, *DMSO, d*), δ=10.39(br.), 9.71(s, 1H, H4), 9.10(d, 2H, H3), 8.82(d, 2H, H5), 8.33-8.25(m, 4H, Hd, Hd′, H1), 8.15(q, 2H, Ha, Ha′), 7.90(t, 2H, Hb, Hb′), 7.80(t, 2H, Hc, Hc′), 7.70(m, 4H, H2, H6).; CHN, Anal. Calc.: ($C_{34}H_{21}N_7O_5S_3Ru$): C, 53.112; H, 3.654; N, 13.281. Found: C, 53.134; H, 3.602; N, 13.312 % .

2. 4. 4. Synthesis of $[Ru^{II}(L)_3](BF_4)_2$*(3).* A mixture of $RuCl_3.xH_2O$ (0.021 g, 0.14 mmol) and (L) (0.1g , 0.42 mmol) in 50 mL ethanol was refluxed under nitrogen atmosphere for 4 h. Then, excess $NaBF_4$ (0.6g) was added and the solution was refluxed for a future 4 h. The resulting precipitate was filtered and washed with ethanol and diethyl ether. The isolated solid was recrystallized from methanol-diethyl ether, after which it was future purified on an alumina column, using acetonitrile/ methanol (2: 1, v/v) as the eluent. Yield 41%.; m. p. >250 °C.; ^{1}H NMR (250 MHz, *DMSO,d*) δ: 10.40(br), 9.70 (s, 2H, H4), 9.0 (d, 4H, H3), 8.85(d, 4H, H5), 8.72-8.67 (m, 6H, Ha, Ha′, H1), 8.20(q, 2H, Hd, Hd′), 8.09(t, 2H, Hb, Hb′), 7.82-7.71(m, 6H, H2, Hc, Hc′), 7.65(t, 4H, H6).; CHN, Anal. Calc.: ($C_{66}H_{39}N_9O_{15}S_3Ru$) : C, 54.187; H, 3.767; N, 9.381. Found: C, 54.202; H, 3.702; N, 9.402%.

2. 4. 5. Synthesis of $[Ru^{II}(bpy)(L)_2](BF_4)_2$*(4).* The complex (4) was prepared, using the same procedure for complex (1) except using 2 equiv (L) (0.1 g, 0.42 mmol) and 1 equiv bpy(0.0018 g, 0.21 mmol). The isolated solid was recrystallized from methanol-diethyl ether, after which it was future purified on a alumina column, using acetonitrile/ methanol (2: 1, v/v) as the eluent. Yield 51%., .m.p. >250 °C. ^{1}H NMR (250 MHz, *DMSO,d*) δ: 10.84(br), 9.70 (s, 3H, H4), 9.0 (d, 6H, H3), 8.72(d, 6H, H5), 8.72-8.34 (m, 6H, H1), 8.0-7.73(m, 12H, H6, H2).; CHN, Anal. Calc.: ($C_{54}H_{34}N_8O_{10}S_2$ B_2F_8Ru) C, 53.635; H, 3.294; N, 9.165. Found: C, 53.605; H, 3.312; N, 9. 202% .

2. 4. 6. Synthesis of $[Ru^{II}(BPhen)(L)(SCN)_2]$ *(5).* The complexes (5) was prepared, using the same procedure for complex(2) except 1 equiv bpy was replaced by 1 equiv BPhen 0.032g (0.016mmol). The product was future purified by column chromatography using alumina as column support and acetonitrile/ methanol (2: 1, v/v) as the eluent. The major dark brown band was collected and corresponds to the desired complex. Yield 40%.; .m. p. >250 °C.; ^{1}H NMR (250 MHz, *DMSO,d*), δ= 10.35(br.), 9.82 (s, 1H, H4), 9.08(q, 4H, H3,Hk), 8.88(d, 2H, H5), 8.76(q, 4H, Hi, H1), 8.66-8.42(m, 6H, Hj, Hj, Hm, Hm′), 8.12(t, 4H, Hn, Hn′), 7.87(q, 4H, Hl, Hl′), 7.73-7.67(m, 4H, H2, H6). CHN analyses of compounds were obtained: Anal. Calc. for (5), ($C_{48}H_{29}N_7O_5Ru$): C, 61. 012; H, 4.034; N, 10.684. Found: C, 61. 077; H, 4.078; N, 10.602% .

3. Results and Discussion

3. 1 Characterization of complexes

The UV–Vis absorption spectra of the ligand(L) and the complexes (1-5) in acetonitrile solution are given in Figure 2.

It can be seen that the absorption bands of ligands appears in the ultraviolet region at around 220-310 nm due to π-π* transitions of the aromatic rings. Free (L) shows three bands at 230, 265 and 305 nm. Moreover, three bands at 218, 260 and 310 nm were observed for bpy. As shown in Figure 2, the absorption spectra of the complexes show the intense bands in the ultraviolet region which can be attributed to the spin allowed π* transitions of the (L) and bpy or BPhen ligands. It

shows that, after coordination the absorption bands are reveal red-shift owing to the formation of the rigid conjugated system after coordination which confirms that the UV spectra of the complexes reflect an essentially absorption of the ligands.

Dalton Transactions Accepted Manuscript

Cite this: DOI: 10.1039/c0xx00000x

www.rsc.org/xxxxxx

ARTICLE TYPE

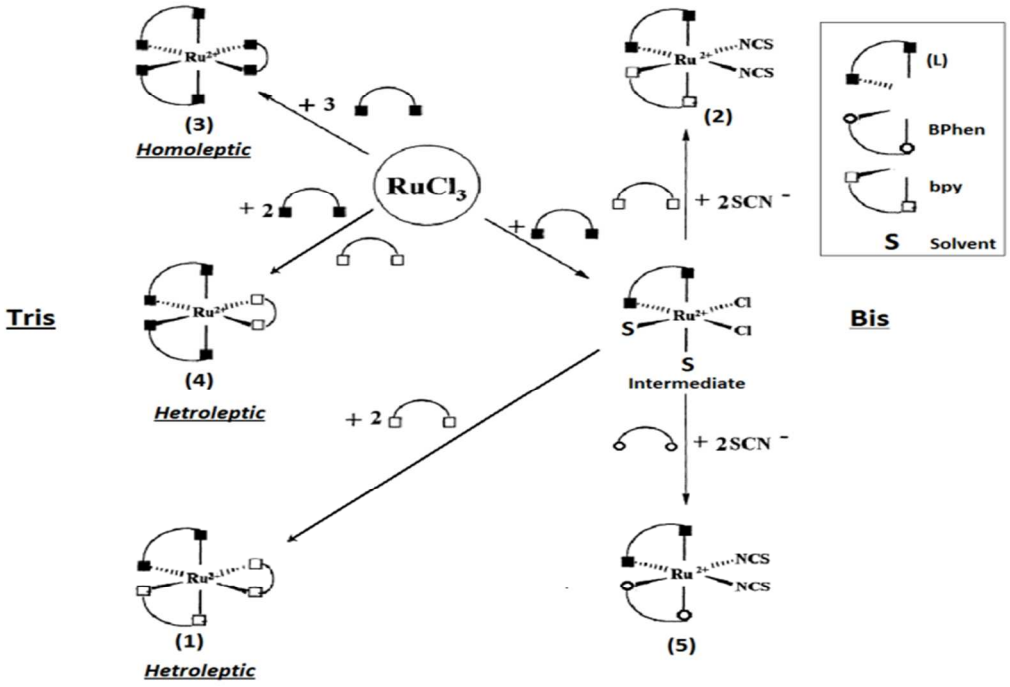

Scheme 2. Schematic representation of different synthetic approaches to Ru(II)-complexes (1-5) .

The broad absorption bands from 400 nm extending to 600 nm corresponds to both spin allowed and spin forbidden metal to ligand charge transfer (MLCT) transitions. The intensity of spin forbidden bands arises from the strong spin orbit coupling of ruthenium (II) which causes the mixing with higher-lying spin allowed transitions.

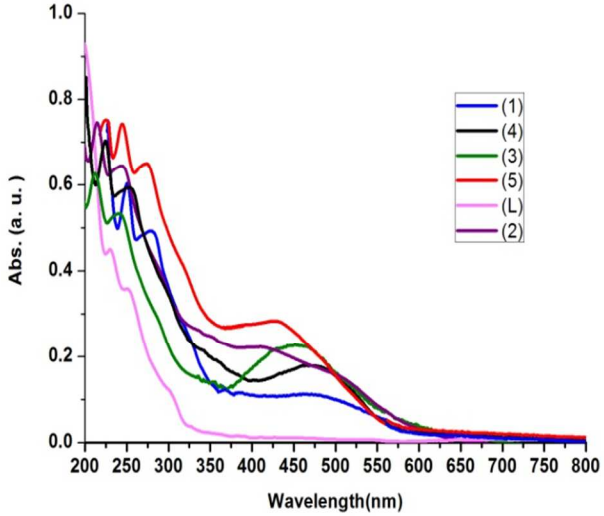

Figure 2. Absorption spectra of ruthenium complexes (1-5) in acetonitrile solution 10^{-5} M.

The PL characteristics of the ruthenium complexes are shown in Figure. 3. The PL emission spectrum of the complex in DMF solution was obtained by exciting the electron with a wavelength of 405 nm. As shown in Figure 3, the Ru complexes emit yellowish-green light at room temperature with emission maximums (l_{em}) at 530 and 570 nm. The broad spectrum indicates that the emissive excited states of complex have more characters of MLCT rather than ligand to ligand charge transfer ($\pi \rightarrow \pi^*$). In figure 3, a red shift and a full-width at half-maximum (FWHM) enhancement of the emission peaks were observed for the complex (2) as compared to the other complexes. Appending aryl sulfonato functionalities also profoundly increases electronic delocalization in the excited state of conjugated systems, inducing significant red-shifts in emission wavelength, and increasing emission intensity. Interestingly, the extended conjugation of the phen ligand at a particular position produced dual emission that was readily resolved in both energy and lifetime [30, 36]. In contrast to compounds (2) and (5), complex (3) exhibited lower luminescent properties than (2) and (5), the additional conjugation to metal center does not seem to have any impact on the coordination complex when three phen aryl sulfonate ligand were coordinated to ruthenium. As our knowledge, this is not the first report of surprising substitution effects at this position of the phen ligand. Wallace et al. discovered that substitution at the 4,7-positions had a far greater impact than any other substitution position on the MLCT energy at room temperature for ruthenium complexes, and reported low-

Dalton Transactions Accepted Manuscript

temperature dual emission of the "distinct orbital type" for these systems [37-39]. In contrast, Yitzhak Tor clearly indicated that both states display the characteristics of ^{3}MLCT states, with regard to energy and excited-state lifetime [36].

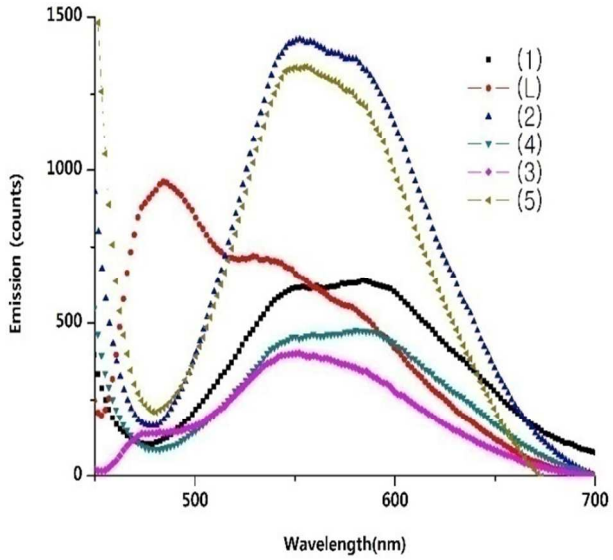

Figure 3. PL spectra of ruthenium complexes (1-5) in DMF solution 10^{-5} M (λ_{exc}=405 nm).

The different photophysical processes in ruthenium polypyridine complexes are summarized in Figure 4. It is useful to note such $dp_{Ru(II)} \rightarrow p^*_{L/bpy}$ based ^{3}MLCT transition band in region 450-550 nm has been observed earlier by many researchers for various Ru(II)–polypyridine complexes [40]. Also, the combination of ^{3}MLCT and ^{3}LLCT absorption bands was responsible for the broad absorption spectrum in the longer wavelength region. In normal ^{3}MLCT emission, the ^{3}MLCT is populated by IC between the S_1 and the ^{1}MLCT and a subsequent ^{1}MLCT- ^{3}MLCT ISC (upon excitation at 400 nm) or by direct ISC between the photoexcited ^{1}MLCT (upon excitation at 525 nm) and the ^{3}MLCT. The crossing of ^{3}MLCT states to lower energetic ^{3}ILCT or ^{3}LLCT excited states, makes the inherent lower energetic of ^{3}ILCT or ^{3}LLCT states with respect to the ^{3}MLCT excited state which leads to photoluminescence in the near-IR region.

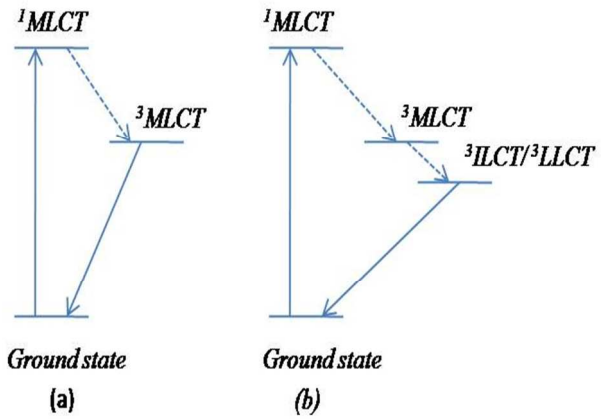

Figure 4. Simplified energy level diagram and the emission states for Ru polypyridine complexes. (a) Normal ^{3}MLCT emission; (b) ^{3} ILCT/ ^{3} LLCT emission.

The internal conversion from ^{3}MLCT to ^{3}ILCT or/and ^{3}LLCT states is reported as a dominant fast phase emission quenching of the ^{3}MLCT state in the sub ns time domain [41]. It is useful to note, the ligand localized CT states (^{3}ILCT or ^{3}LLCT) emission is too low to observe in emission spectroscopy at room temperature [42]. Earlier, the ^{3}MLCT→ ^{3}ILCT internal conversion is reported to be as fast as~100 ps by Charlot et al [43]. Generally, ruthenium polypyridine complexes exhibit long ^{3}MLCT lifetimes from milli second to micro second. As an example, a family of Ru(II) complexes containing substituted 1,10-phenanthroline ligands with extended conjugation display two simultaneously emissive ^{3}MLCT excited states in solutions at room temperature, originating from bpy-based (t= 0.9 to 2.2ms) and longer lived phen-based (t= 3.7 to 11.5ms) excited states [44]. Therefore, the assignment of ^{3}ILCT and ^{3}LLCT to emission bands at centered 570 nm will be ruled out and ^{3}MLCT $\rightarrow S_1$ will be reasonable.

The main absorption peaks in the IR spectra of complexes (1-5) are summarized in Table 1. Generally, in the IR spectrum of the phen, strong bands were observed in frequency region between 1400 and 1650 cm^{-1}, the one band occurring at 1505 cm^{-1}, the second appearing at 1590 cm^{-1} and the third band at 1423 cm^{-1}.

Table 1. The main absorption peaks in the IR spectra of complexes (1-5), (cm^{-1}).

Dye	$\nu(SO_3)_{sym}$	$\nu(SO_3)_{assym}$	ν(O-H)	ν(SCN)	ν(C-H)	$\nu(C=N)_{imin}$	ν(C=O)
L	1090	1290	3400	-	2922	1704	1684
(1)	1069	1299	3400	-	2918	1699	1625
(2)	1043	1255	3414	2097	2918	1689	1632
(3)	1036	1226	3406	-	2919	1707	1632
(4)	1043	1298	3412	2088	2920	1728	1632
(5)	1052	1241	3410	-	2919	1692	1626

In the present study, IR spectra of (L) show ν(C –N) band related to phen, at 1422 cm^{-1}, indicating the partial double bond character. The ring frequencies associated with phen are observed at 1497, 1601 cm^{-1} for (L). The ν(C –H) of phen bands appear at 2876, 2946, 2965 cm^{-1}. In aryl sulfonyl ligand (L), bands at 1290, 1090, 684 and 561 cm^{-1} derive from presence of SO_3. The vibration band at 1030-1090 cm^{-1} is characteristics of the vibrations of the sulfur atoms linked to the aromatic cycle and of S=O symmetric [45]. The asymmetric S=O vibration is observed at 1220-1290 cm^{-1}. It is important to note, the disappearance of $\nu(NH_2)$ stretching frequency of amine group and appearance of ν(NH) stretching at 3445 cm^{-1} in the IR spectrum of (L) reveals the formation of (L). The region of particular interest is between 1800 and 1000 cm^{-1}, as the various C-O stretching bands which are found here indicate the types of C-O bonding which are present in the molecule. This region is complicated with vibrations of the bpy framework; sulfonate groups all contributing to the spectra. In the IR spectra of complexes (1-5), strong peak at 2918-2922 cm $^{-1}$ for complexes (1-5) were assigned to the (C-H) group, and a strong absorption at 1220-1290 cm $^{-1}$ for all complexes (1-5) corresponds to the $\nu(SO_3)$ vibration of the sulfonate group. The NCS –group has two characteristic modes, ν(NC) and ν(CS), which are frequently considered as diagnostic with respect to the coordination mode of the ambidentate NCS ligand. The IR spectra of complexes (2 and 4) show an intense absorbance at 2088 cm $^{-1}$ and 2097 cm $^{-1}$ ν (NC) and 780 and 785 cm $^{-1}$ ν(CS) due to the N-coordinated NCS ligand. There are a number of bands to lower energy (to1000 cm^{-1}) in dyes which contain both C-C, C-N, S-O stretching and S-O deformation character Further information on the complexes was obtained from ^{1}H-NMR spectroscopy. ^{1}H-NMR spectra of all complexes show all peaks of synthesized ligand(L) , bpy, phen and BPhen at region 7.5 -10.8 ppm that indicate the presence of ligands in complexes. The signal integration for complex (1)

Dalton Transactions Accepted Manuscript

reveals the incorporation of one (L) and two bpy units. For complex (2), two (L) units and one bpy unit were found by signal integration. Three and two (L) units were revealed by signal integration for complexes (3) and (4), respectively. The signal integration for complex (5) reveals the incorporation of one BPhen and two (L) units. The difference between the chemical shift of free ligands and complexes indicates that the coordination of ligands to metal is occurred. The cyclic voltammograms of complexes (1-5) show the features characteristic for ruthenium-polypyridine complexes, with a reversible metal based oxidation (Ru^{III}/Ru^{II}) at positive potentials from +1.2 (V) to +1.4 (V) and four quasi-reversible reductions at negative potentials from -1.1 (V) to-1.9 (V) (ESI†, S2). The first reduction wave is due to the reduction of the sulfonyl ligand, and is followed, at more negative potentials, by three successive electron reduction of the bpy or phen ligands [46] . The LUMO and HOMO of the ground state of dyes (1-5) are about 2.8-3.8 and 3.0-4.5 V versus NHE. These energy levels of LUMO and HOMO are able to inject energetically electrons into the conduction band of TiO_2 and accept electrons from iodide ions, respectively.

3.2 EL characterization

Figure 5 shows the EL spectra of PVK: PBD and ruthenium complexes (1-5) in PVK: PBD blend. An emissive layer without ruthenium complex was fabricated to record the PVK: PBD EL spectra and to find a relation between EL spectra of ruthenium compounds and PVK: PBD EL in order to separate it from the emission of ruthenium complexes (Figure 5). In the EL spectra, ruthenium complexes show a long red shift rather than PVK: PBD EL spectra, demonstrating that effective energy transfer is taking place in the emissive layer. As the driving voltage is biased to electrodes, the electrons and holes begin to inject into bulk. Some of electrons and holes under the electromagnetic forces form excitons, which emit light with their anelation between HOMO and LUMO energy levels of layers.

To achieve a good balance of holes and electrons, both hole and electron-transporting functions (PVK: PBD) incorporated into a single Ru emiter. It should be noted that our results show high ratio of PBD leads to lower stability of the device due to the decrease in the ratio of PVK.

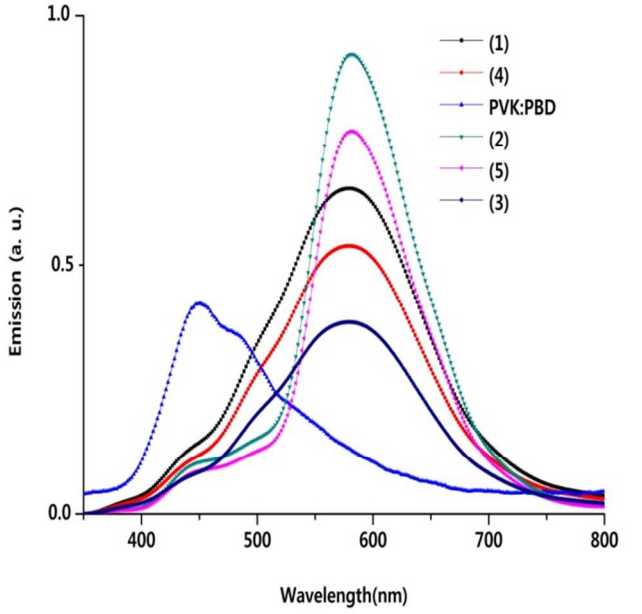

Figure 5. EL spectra of PVK: PBD and ruthenium complexes (1-5) in PVK: PBD blend.

However, the ruthenium devices made without PBD in the blend layer is weak electroluminescent and PVK is the dominant emitter. Finally, the efficient ratio of 10: 4: 1 for PVK: PBD: dye was suggested, which reduces the risk of excimer formation and increases the stability of the device. The use of PEDOT: PSS interlayer helps also better hole injection into emissive layer that results in increasing current and probability of exciton formation.

The formation of Forster transfer is possible in Ru complexes since there is overlap between the absorption spectra of dyes and emission spectra of PVK: PBD. Moreover, the arrangement of layers was caused the Forster transfer of energy was resulted from PVK: PBD host to ruthenium complexes (Figure 6). This arrangement indicates that the NCS ligand can be directly affect the position of the HOMO energy level which the HOMO is delocalized over the NCS ligands. As shown in Figure 6, these arrangements of energy level also allow to ruthenium complexes insides into electron transport layer (PBD) and hole injector layer (PVK). As shown in Figure 5, the device (2) gives the highest EL efficiency than that of other devices. The maxima of EL for Ru complexes (1-5) were centered at 580 nm. The electroluminescence spectrum results in CIE color coordinates of x = 0.51 and y= 0.41 for dyes (2) corresponding red emission. Figure 7 shows the variation of current density with respect to voltage increase. As shown in Figure 7, all devices show rapid growth in current densities at voltages more than 8 V. It means that at this voltage the potential barrier for charge injection is overcome by the electric field exerted between anode and cathode, and helps to rise in the current density. In addition, at specified voltage for example 15 V, sample (2) has the highest current density compared to others. In addition, at higher voltages, it is obvious that all samples depict relatively same behavior in current density change with voltage.

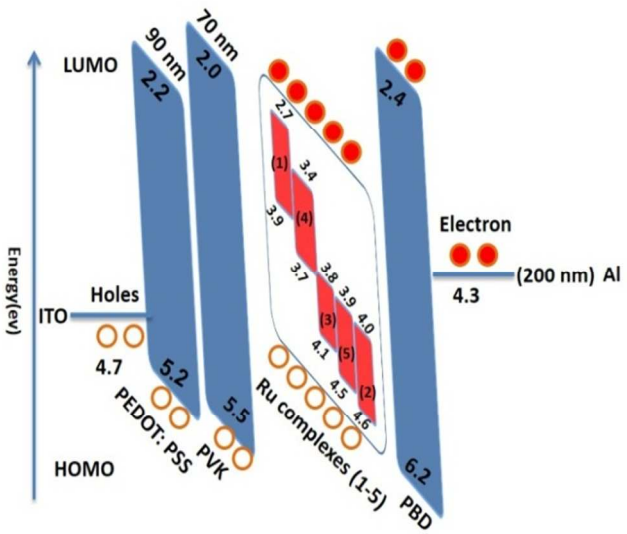

Figure 6. Schematic showing the energy levels of device and the dynamic process of EL emission.

The device (2) also has a luminance of 550 cd/m^2 and maximum efficiency of 0.9 cd/A at 18 V which are the highest values among the five devices. Figure 8 shows the maximum efficiency (LE) versus applied voltages (V) characteristics of Ru devices (1-5). The turn-on voltage of this device is approximately 5 V. For device (2), the full width at half-maximum (FWHM), and the

Dalton Transactions Accepted Manuscript

This journal is © The Royal Society of Chemistry [year]

correlated color temperature (CCT) at 18 (V) were 103 nm and 2145(K), respectively.

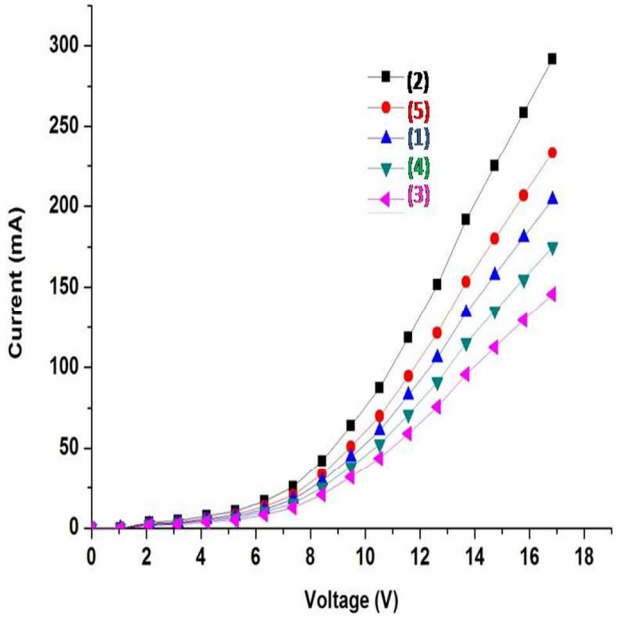

Figure 7. Current density versus applied voltage for devices (1-5).

The obtained LED performance of sample (2) is acceptable data among reported Ru complexes for future investigations. Table. 2 summarized the color coordinates in the Commission Internationaledel'Eclairage (CIE 1931) chromaticity chart, the full width at half-maximum (FWHM) and the correlated color temperature (CCT) for complexes (1-5), (L) and PVK:PBD.

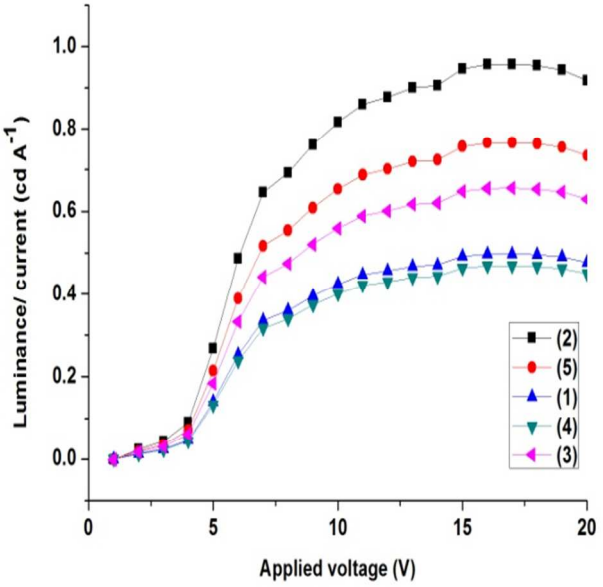

Figure 8. The maximum efficiency (LE) versus applied voltages (V) characteristics of Ru devices (1-5).

Table. 2: The color coordinates in the Commission Internationaledel' Eclairage (CIE 1931) chromaticity chart and the full width at half-maximum (FWHM) and the correlated color temperature (CCT).

Dye	CIE	FWHM(nm)	CCT(K)
(1)	x = 0.4461 y = 0.4298	158	3054
(2)	x = 0.5117 y = 0.4183	103	2145
(3)	x = 0.5117 y = 0.4183	103	2145
(4)	x = 0.5117 y = 0.4183	103	2145
PVK:PBD	x = 0.2707 y = 0.2968	115	9471
(5)	x = 0.4461 y = 0.4298	158	3054
(L)	x = 0.4461 y = 0.4298	158	3054

3. 3 DFT calculation. DFT calculations were also performed to aid in the interpretation of the role of the ligands to electron transfer mechanisms of Ru complexes. The optimized structures of the different donor and acceptor moieties of the ruthenium complexes used in this study are shown in Figure 9.

Figure 10 shows the five highest and five lowest molecular orbital energy levels of the Ru complexes. Note that the LUMO energy level of the complex (1) contain two bpy groups is relatively higher than those of the other complexes, with an estimated value of 0.70-1.3 eV, and that the HOMO energy level is relatively higher than those of the other complexes with a difference of approximately 0.605-1.21 eV. This makes the HOMO–LUMO gaps of the complexes (2-5) models smaller compared to complex (1). The presence of synthesized ligand(L) in the ruthenium complexes decreases the HOMO–LUMO gap. Another interesting feature found in Figure 10 is the minimal difference in the bpy ligand of their HOMO and LUMO levels.

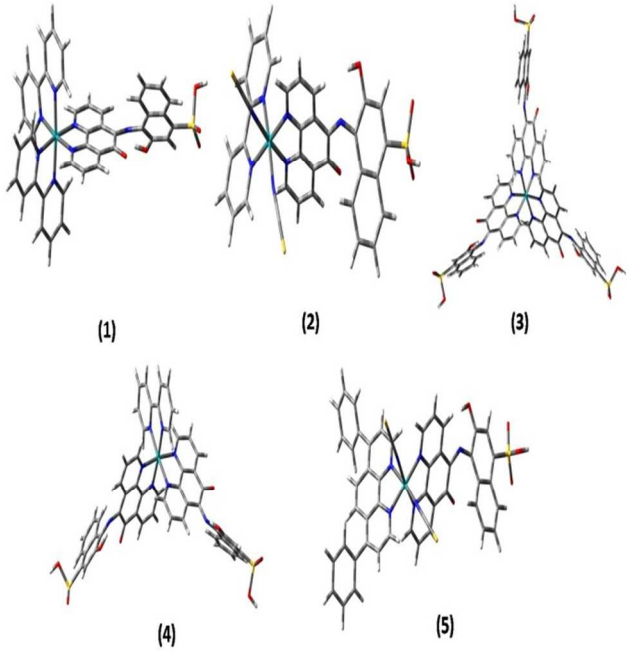

Figure 9. Optimized structures of novel ruthenium complexes (1-5).

The bpy ligand have almost low influence on the HOMO and LUMO levels in complex (1), which is in congruence with the theoretical results of our group. For the acceptor moiety, sulfonic acid is the main functional group, and it is an anchoring functional group for titanium dioxide. Similar exist

Dalton Transactions Accepted Manuscript

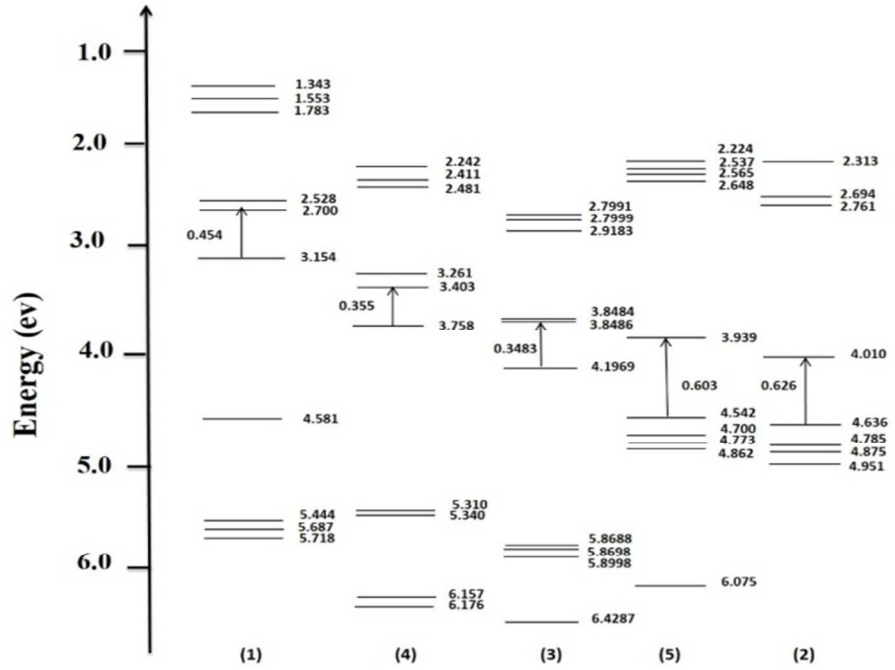

Figure 10. Diagram of the three highest occupied and three lowest unoccupied molecular orbital levels of novel ruthenium complexes (1-5).

in the structure of the chosen acceptor moieties. The presence of such additional 1-naphthalene carboxylic acid group decreased their LUMO energy levels considerably relative to three (1-naphthalene sulfonic acid) group in complex (3) by approximately 0.694 eV than that of complex (1). Overall, complex (1) had the highest LUMO level and complexes (2 and 5) had the lowest LUMO level, with a 1.3 eV difference relative to each other. The relative positions of the LUMO levels for the donor and acceptor moieties are very important for charge transport to be effective [47, 48]. Comparing the LUMO levels of the donor moieties complexes (1 to 5) with those of the acceptor moiety would show that the donor complex (1) moiety have LUMO level higher than acceptor moiety complexes (2) and (5). Complex (1) has higher LUMO level relative to the complexes (2), to (5) acceptor moiety. The donor and acceptor moieties cited above have a LUMO donor–LUMO acceptor
difference that ranges from approximately 0.35–0.62 eV, which is sufficient for charge transport. Figure 11 shows the HOMO and LUMO orbital spatial orientation of the novel ruthenium complexes (1-5). Mizuseki et al. [49] suggested that the charge transport was related to the spatial distribution of the frontier orbitals. The HOMO should be localized in the donor moiety and the LUMO in the acceptor moiety [50, 51]. Regarding the HOMO-LUMO gap in the $[RuL]^{2+}$ complexes, it appears in the order $[Ru(L)(bpy)(SCN)_2]$ (2) ~ $Ru(L)(BPhen)(SCN)_2](BF_4)_2$ (5)> $[Ru(L)(bpy)_2](BF_4)_2$ (1) ~ $[Ru(L)_3](BF_4)_2$ (3) ~ $[Ru(L)_2(bpy)](BF_4)_2$ (4). With considering HOMO-LUMO gap, the common features of the UV-Vis absorption spectra are: (i) The MLCT transitions are hypsochromically shifted upon the presence of SCN ligand, ranging from 440 nm for (2) to 485 nm for (3). On the other hand, Π-conjugated ligand is bathochemically shifted MLCT transition. (ii) Broad bands in the visible region corresponding to the envelope of the Ru–bpy/BPhen and Ru–L MLCT transitions. It is useful to note the status of HOMO and LUMO levels of complexes is important to electron injection in OLED and DSSC. The best match between LUMO level of dye and the conduction band of TiO_2 has achieved by complex (2). So, we conclude that the presence of bpy and SCN is the best configuration for DSSC based solfunat anchoring group.

In our calculations, complex (1) with donor having higher LUMO level have their HOMO localized in the donor and acceptor regions and their LUMO localized in the donor region. Complexes (2) and (5) have (-NCS) groups in their structure, which caused the localization of the LUMO in the acceptor region. The HOMO of structure (1) is localized in the donor moiety and the LUMO is mostly in the same region. The same trend was observed for the orbital spatial orientation of ruthenium complex analogues, as shown in Figure 11. The presence of ruthenium metal might be responsible for the delocalization of both the HOMO and LUMO, suggesting the presence of a metal-to-ligand charge transfer (MLCT) or metal-centered transitions from both the metal and the ligand p orbitals in the LUMO [52]. Another noteworthy feature in figure 10 is the effect of the present of (-NCS) groups in the donor moiety of structures (2) and (5). The electron-donating of (-NCS) groups seem to localize the HOMO on their side. This is very evident in the structures (2) and (5) contain of (-NCS) groups donor moieties. Figure 11 also shows the HOMO and
LUMO levels for the novel ruthenium complexes analogues. The structures (3) and (4) analogues have smaller HOMO–LUMO gaps compared to the other complexes with a difference of approximately 0.12–0.32 eV.

The results of the calculations revealed that the HOMO and LUMO values of both the structures (3) and (4) analogues are

Dalton Transactions Accepted Manuscript

This journal is © The Royal Society of Chemistry [year]

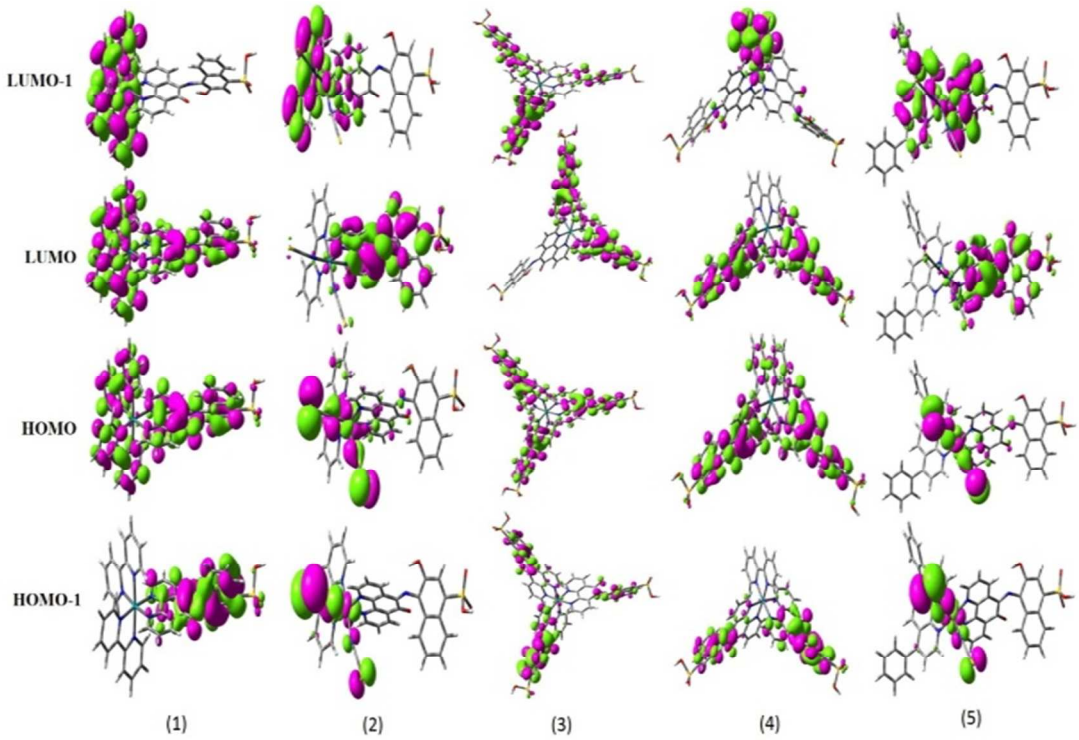

Figure 11. Molecular orbital spatial orientation for complexes (1-5).

roughly the half HOMO and LUMO values of the structures (2) and (5), as shown in Figure 11. It also shows a trend in the combination of donor moieties with that of the acceptor moieties: if both have small HOMO–LUMO gaps, the donor–acceptor moieties would be more likely to have small HOMO–LUMO gaps. This trend is clearly observed in the structures (2) and (5) donor moiety and the structure (3) acceptor moiety, which has the lowest gap among the moieties studied.

3.4 DSSC measurements.

The photovoltaic performances of Ru (1-5) measured under identical conditions are summarized in Table 3. Figure 12 shows comparison of the J–V measurement results of complexes (1-5) used in the solar cells. Complex (2) showed the highest short circuit current and fill factor among dyes. Spectral characteristics of the investigated dyes are similar. It is clear from the data that dye (2) is the most efficient sensitizer of the all dyes. Indeed, the efficiencies of the DSSCs prepared with classical type of $Ru(bpy)(SCN)_2(L)$ which (L) has bearing sulfonyl acid, significantly (i.e. 10 times) higher than those of the none classical dyes. The J_{sc} value increased in the following order: (2)>(5)> (1) >(4) > (3).

Two SCN substituent yielded a higher J_{sc} for the cell than tris ligand(L) substituent. This indicates that the addition of NCS ligands influences on the cell performance. The effect of anchoring group number on the performance of DSSC is critical in achieving high efficiency. Hara et al. found that a monocarboxylate Ru-phen complex was less efficient than that obtained using di- or tricarboxylate [53, 54].

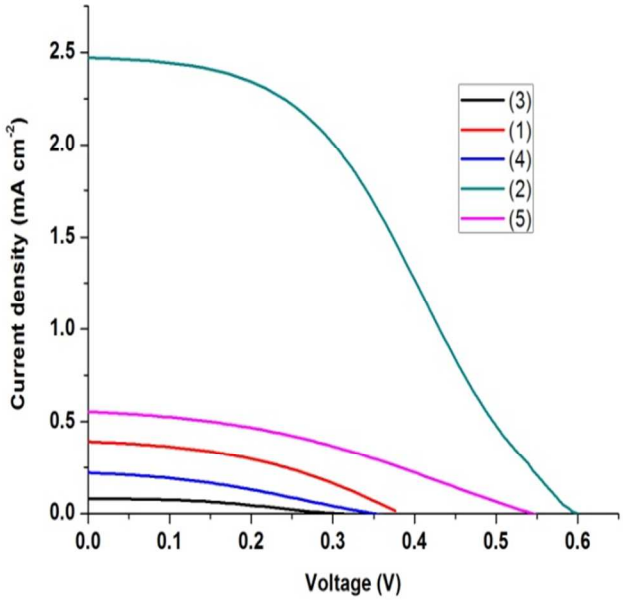

Figure 12. I−V curves of DSSCs sensitized with complexes (1-5).

Yang et al. found that in triphenylamine-based, multiple rhodanine-3-acetic acid electron acceptor dyes, those which contained two anchor groups (rhodanine-3-acetic acid) exhibited superior photovoltaic performance than those with one or three anchor groups, owing to red shifts and broadening of absorbance [55]. H. Shang et al. indicated the more anchoring groups the dye has, the lower efficiency the device exhibits [56]. Here, the efficiencies of the DSSCs are susceptible to changing the number of anchoring groups/sulfonyl groups in the dyes. Increasing

Dalton Transactions Accepted Manuscript

anchor group number resulted in lower short-circuit current and lower efficiency. Dye (2) showed the highest J_{sc} value compared to the other dyes for three main explanation: The dye solution of complex with more sulfonyl group may contain hydrogen-bonded aggregates on the surface that prevent penetrating into the small pores of the TiO_2 surface. Besides the hydrogen-bonded aggregates, the orientation of adsorbed sensitizer on the surface may also be responsible for lower surface concentration of the dye. The other possible explanation is that the rate of regeneration of dyes with more anchoring group with I^-/I^{3-} is slower than with complex (2) since the presence of NCS groups on complex(2) accelerates the regeneration [57]. This will directly impact the number of electrons being injected that will consequently influence the J_{sc}. Another reason to fail compounds (1), (3) and (4) for our aim is they have no dye regeneration process as their HUMO energies lie high above the redox level of electrolyte. As shown in Figure 12, the best energy level alignment among HOMO-LUMO of dye, electrolyte and conduction band of TiO_2 was occurred for dye (2) and (5). It is very important to note, when one of the bidentate ligands of $[Ru(bpy)_3]^{2+}$ is replaced by two NCS ligands, the lower symmetry of the complex compromises the degeneracy of the MLCT transitions to lead to a broader absorption band [58]. The installation of the two NCS ligands also raises the energy of the HOMO resulting in a bathochromic shift of the low-energy MLCT band [59].

Table 3. Photovoltaic performances of DSSCs sensitized with (1-5) and Ru sulfonated bipyridine (1-3b and 3e) :(radiant power: 27 mW/cm^2(AM 1.0 direct); Red /Ox electrolyte NMO, LiI (0.5 M), I_2 (0.5 mM) and 4-tert-butylpyridine (100 mM).1b; $[Ru(dsbpy)_3]^{2+}$, 2b; $[Ru(dmbpy)_2(dsbpy)]^{2+}$, 3b; $[Ru(dsbpy)_2Cl_2]$, 3f; $[Ru(dsbpy)_2(NCS)_2]$. (Where (dmbpy)=4,4′-dimethyl-2,2′ -bipyridine, and $(dsbpy)_2$= 2,2′ -Bipyridine-4,4′ disulfonic acid).

Dye	J_{sc}(mA/cm^2)	V_{oc}(V)	FF(%)	η(%)	IPCE(%)	Ref
(1)	0.39	0.37	20	0.03	7	This work
(2)	2.46	0.6	40	0.67	23	This work
(3)	0.07	0.28	12	0.003	2	This work
(4)	0.22	0.34	14	0.01	5	This work
(5)	0.54	0.53	21	0.07	9	This work
1b	1.4	0.52	34	0.9	-	60
2b	1.3	0.53	37	0.9	-	60
3b	1.3	0.51	42	1.1	-	60
3e	0.5	0.52	36	0.4	-	60

Figure 13 shows the operating principles and energy level diagram of dye-sensitized solar cell for complexes (1-5). FT-IR spectroscopy has been shown to be a powerful tool for extracting structural information of the molecules adsorbed onto a TiO_2 surface. Figure 14 shows FT-IR spectra of ruthenium complex (1) and ruthenium complex (1) adsorbed on TiO_2 films. The region of particular interest is between 1000 and 1300 cm^{-1}, as the various S-O stretching bands which are found here indicate the types of S-O bonding which are present in the molecule.

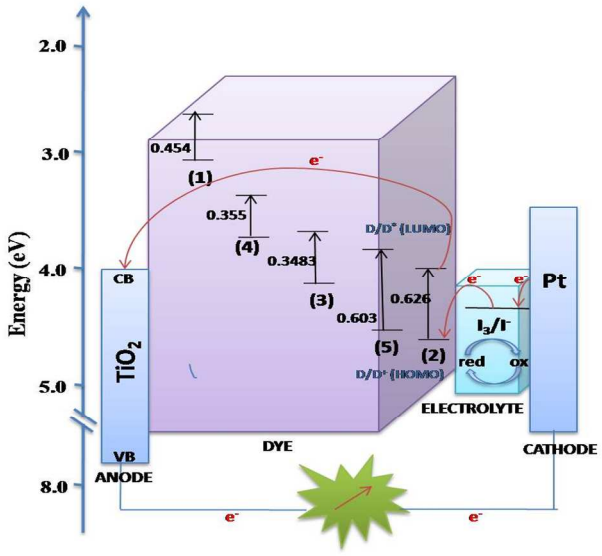

Figure 13. Operating principles and energy level diagram of dye-sensitized solar cell for complexes (1-5).

This region is complicated with vibrations of the bpy and aryl circle framework all contributing to the spectra. There are a number of bands to lower energy (to 1000 cm^{-1}) in dyes and dyes anchored to TiO_2 which contain both C-C and C-N stretching, S-O stretching and SO_3 deformation character.

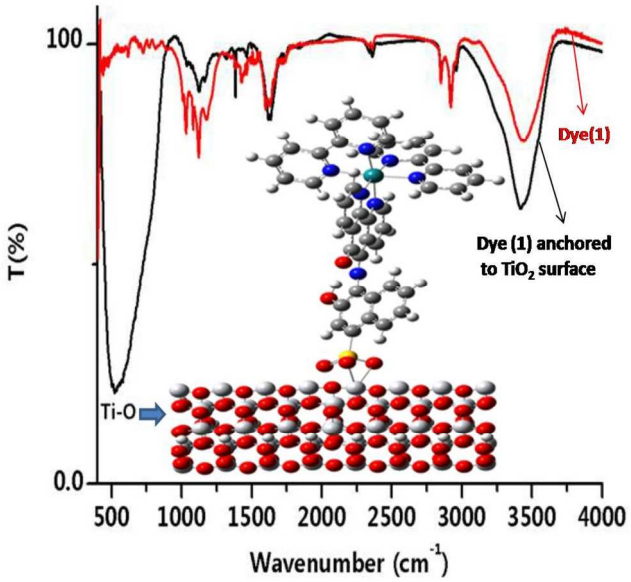

Figure 14. FT-IR spectra of ruthenium complex(1) (redline) and ruthenium complex(1) adsorbed on TiO_2 films (black line). Inset: TiO_2-anatase nanostructures extended along the [101] directions sensitized by dye (1).

The other prominent band at 500 cm^{-1} in anchored Ru onto TiO_2 is due to (Ti-O) stretching band of TiO_2 surface. For all dyes adsorbed on TiO_2, there is an intense, broad band at region 1200-1300 cm^{-1} (overlapping the highest bpy band), which is assigned to the anti symmetric stretch of $-SO_3^-$, where the negative charge is delocalized to give two equivalent (or nearly so) S-O bonds. There is a high-energy tail to the band indicating some variation in this bonding. The other intense band in this spectrum at 1050-1150 cm^{-1} is assigned as the symmetric stretch of $-SO_3^-$, since it is not assignable to the polypyridine ligands [61-63]. The

Dalton Transactions Accepted Manuscript

This journal is © The Royal Society of Chemistry [year]

difference between $\nu_{as}(SO_3)$ and $V_s(SO_3)$ ($\Delta\nu$), compared to the corresponding values in ionic (94 nm), is currently employed to determine the corresponding mode of the sulfonat group. The possible binding modes for ruthenium polypyridine containing sulfonato group on a TiO_2 surface are shown in Figure 15.

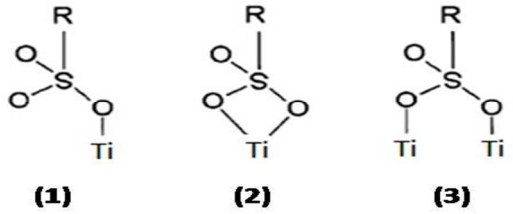

Figure 15. Possible coordination modes for sulfonate anions in the TiO_2 solid state.

1. The unidentate coordination of the sulfonato group removes the equivalence of the three oxygen atoms, resulting in an ester type of bond formation between the sulfonato group and the TiO_2 surface. Unidentate complexes (figure 15(1)) exhibit the $\Delta\nu$ values [$\nu_{as}(SO_3^-) - \nu_S(SO_3^-)$] which are much greater than the ionic complexes. 2. Chelating complexes (figure 15(2)) exhibit $\Delta\nu$ values which are significantly less than the ionic values. 3. The $\Delta\nu$ values for bridging complexes (figure 15(3)) are greater than those of chelating complexes, and close to the ionic values On the basis of the FT-IR measurements, the difference between the $\nu_{as}(SO_3^-)$ and $\nu_s(SO_3^-)$ in the Ru complexes (90-100 cm^{-1}) and the adsorbed Ru complexes (85-110 cm^{-1}) suggest that's the sulfonato group are bound to the TiO_2 surface via chelating mode (2).

Action spectrum, incident photon-to-electron conversion efficiency (IPCE) as a function of wavelength, was measured to evaluate the photoresponse of photoelectrode in the whole spectral region. Figure 16 shows the IPCE spectra of DSCs based on dyes (1-5). All five dyes can convert visible light to photocurrent in the range of 400-700 nm. In the range of 400-500 nm, IPCE maxima of up to 7%, 23%, 2%, 5%, 9% were achieved for dyes (1-5), respectively. Dye (2) gave broader spectra and higher photoresponse in the long wavelength region (>500 nm) than other dyes, which was consistent with the corresponding absorption spectra on transparent TiO_2 film.

According to the photocurrent action spectra, one may expect higher short-circuit photocurrent densities (J_{sc}) for dye (2)-based DSCs from the overlap integral of IPCE curves with the standard AM 1.5 solar emission spectrum. Indeed, dye (2)-based DSCs give higher J_{sc} (2.46 mA/cm^2) than other samples (see Figure 16 and Table 3), which is consistent with the IPCE data. The sensitizer with more sulfonyl acid anchoring groups upon adsorption transfers more protons to the TiO_2 surface, leading to the positive shift of the conduction band edge of TiO_2.

Thus, the increasing of the sulfonyl acid anchoring groups could lead to increased charge recombination at the TiO_2/dye/electrolyte interface and lower efficiency [64].

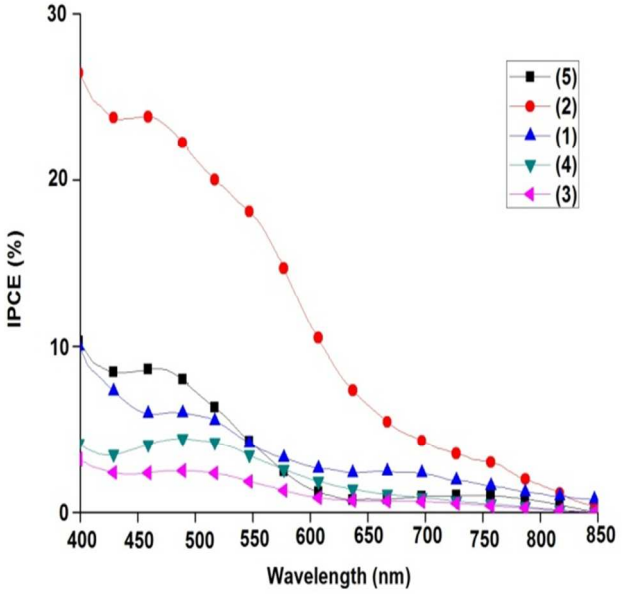

Figure 16. Photocurrent action spectra of nanocrystalline TiO_2 films sensitized by complexes (1-5). The incident photon-to-current conversion efficiency is plotted as a function of wavelength.

Further works on ruthenium complexes with other polypyridin ligands are in progress, and we believe that the improvement can be accomplished by a thorough replacement of the attached functionalized groups to the ruthenium complexes in both DSSC and OLED fields.

4. Conclusion

Synthesis of new hetroleptic and homoleptic ruthenium(II) complexes with Π-extended phenantroline sulfonate derivates and its application in both light emission diode and dye-sensitized solar cells have been reported. This is interesting because the work mechanism of above two devices is nearly inversed. We obtained better efficiency of both DSSCs and OLEDs prepared with dye (2) in comparison to that with other dyes under standard conditions. Increased electron injection is reflected in the increased short-circuit photocurrent density (J_{sc}) and overall efficiency. DSSC and OLED studies reveal that ruthenium polypyridine with NCS ligand exhibits better current generating capacity than the ruthenium polypyridine without NCS groups. DFT calculations also show that complexes (2) and (5) have (-NCS) groups in their structure, which caused the localization of the LUMO in the acceptor region. The EL spectra of ruthenium complexes were indicated a long red shift in visible region rather than PVK: PBD blend. This characteristic together with favorable electronic and redox properties as demonstrated by DFT calculation, optical and electrochemical studies make $Ru(L)(bpy)(SCN)_2$(2) where L= 6-one-[1,10]phenanthrolin-5-ylamino)-3-hydoxy naphthalene 1-sulfonic attractive for further photoelectric applications. To our knowledge, this class of dyes has not been previously reported, and this finding opens the pathway to designing dyes that both absorb the visible light for conversion solar to electricity and light emission by further modification of the ligand architecture, which will improve notably power conversion efficiencies of dye-sensitized solar cells and efficient light emission diodes.

References

Dalton Transactions Accepted Manuscript

(1) B. O'Regan, M. Gratzel, *Nature*, 1991, **353**, 737.
(2) J. M.Rehm, G. L. McLendon, Y. Nagasawa, K. Yoshihara, J. Moser, M. Gratzel,. *J. Phys. Chem. lett.,* 1996, **100** , 9577.
(3) A. Hagfeldt, M. Gratzel, *Chem. Rev*., 1995, **95**, 49.
(4) M. Gratzel, *Nature*, 2001, **414**, 338.
(5) M. K. Nazeeruddin, Q. Wang, L. Cevey, V. Aranyos, P. Liska, E. Figgemeier, C. Klein, N. Hirata, S. Koops, S. Haque, J. R. Durrant, A. Hagfeldt, A. B. P. Lever, M. Gratzel, *Inorg. Chem*., 2006, **45**, 787.
(6) P. V. Kamat, *J. Phys. Chem. C*., 2007, **111**, 2834.
(7) C. Adachi, M. A. Baldo, M. E. Thompson, S. R. Forrest, *J. Appl. Phys*. 2001, **90**, 5048.
(8) M. A. Baldo, S. Lamansky, P. E. Burrows, M. E. Thompson, S. R. Forrest, *Appl. Phys. Lett.* 1999, **75**, 4.
(9) M. Ikai, S. Tokito, Y. Sakamoto, T. Suzuki, Y. Taga, *Appl. Phys. Lett*., 2001, **79**, 156.
(10) M. K. Nazeeruddin, R. Humphry-Baker, D. Berner, B. S. Rivier, L. Zuppiroli, M. Gratzel, *J. Am. Chem. Soc*. 2003, **125**, 8790.
(11) W.S. Han, J. K. Han, H. Y. Kim, M. J. Choi, Y .S .Kang, C . Pac, S. O. Kang, *Inorg. Chem.*, 2011, **50**, 3271.
(12) M. K. Nazeeruddin, A. Kay, I. Rodicio, R. Humphry-Baker, E. Mueller, P. Liska, N. Vlachopoulos, M. Graetzel, *J. Am. Chem. Soc*., 1993, **115**, 6382.
(13) C. A. Bignozzi, R. Argazzi, C. Kleverlaan, *Chem. Soc. Rev*., 2000, **29**, 87.
(14) Md. K. Nazeeruddin, S. M. Zakeeruddin, J. J. Lagref, P. Liska, P. Comte, C. Barolo, G. Viscardi, K. Schenk, M. Gratzel, Coord. Chem. Rev., 2004, **248**, 1317.
(15) E. A. M. Geary, L. J. Yellowlees, L. A. Jack, I. D. H. Oswald, S. Parsons, N. Hirata, J. R. Durrant, N. Robertson, *Inorg. Chem*., 2005, **44**, 242.
(16) Z. Wang, F. Li, C. Huang, L. Wang, M. Wei, L. Jin, S. Tian, N. Li, *J. Phys. Chem. B.* 2000, **104**, 9676.
(17) S. Y. Liu, Z. K. Chen, L. H. Wang, E. T. Kang, Y. H. Lai, S. J. Chua, W. Huang, *Synth. Met*., 2000, **114**, 101.
(18) Z. Wang, F. Li, C. Huang, *J. Phys. Chem. B,* 2001, **105**, 9210.
(19) P. Falaras, *Sol. Eng. Mat. Sol, Eng*., 1998, **53**, 163.
(20) K. Murakoshi, G. Kano, Y. Wada, S. Yanagida, H. Miyazaki, M. Matsumoto, S. Murasawa, *J. Electroanal. Chem*., 1995, **396**, 27.
(21) T. J. Meyer, G. J. Meyer, B. W. Pfennig, J. R. Schoonover, C. J. Simpson, J. F. Wall, C. Kobusch, Y. Chen, B. M. Peek, C. G. Wald, W. Ou, B. W. Erickson, C. A. Bignozzi, *Inorg.Chem*., 1994, **33**, 3952.
(22) P. Falaras, I. M. Arabatzis, T. Stergiopoulos, G. Papavassiliou, M. Karagianni, *J. Mater. Process. Technol .,* 2005, **61**, 276.
(23) N. Tokel, A. J. Bard, *J. Am. Chem. Soc*., 1972, **94**, 2862.
(24) R. S. Glass, L. R. Faulkner, *J. Phys. Chem.,* 1981, **85**, 1160.
(25) I. Rubinstein, A. J. Bard, *J. Am. Chem. Soc*., 1981, **103**, 512.
(26) F. Kanoufi, A. J. Bard, *J. Phys. Chem. B,* 1999, **103**, 10469.
(27) A. Juris, V. Balzani, F. Barigelletti, S. Campagna, P. Belser, A. V. Zelewsky, *Coord. Chem. Rev*., 1988, **84**, 85 .
(28) I .Rubinstein, A. J. Bard, *J. Am. Chem. Soc.,* 1980, **102**, 6641.
(29) A. J. Bard, J. D. Debad, J. K. Leland, G. B. Sigal, J. L. Wilbur, J. N. Wohlstadter, Encyclo. Anal. Chem, ed. R. A. Meyers, Wiley, Chichester. **2000**, p. 9842.
(30) H. Rudmann, M. F. Rubner, *J. Appl. Phys*., 2001, **90**, 4338.
(31) H. Rudmann, S. Shimada, M. F. Rubner, *J. Am. Chem. Soc.,* 2002, **124**, 4918.
(32) M. Thelakkat, H. W. Schmidt, *Adv. Mater*., 1998, **10**, 219.
(33) R. S. Ashraf, M. Shahid, E. Klemm, M. Al-Ibrahim, S. Sensfuss, *Macromol. Rapid. Commun*., 2006, **27**, 1454.
(34) M. J. Frisch, G. W. Trucks, H. B. Schlegel, , G. E. Scuseria, M. A. Robb, J. R.Cheeseman, J. A. Montgomery, T. Vreven, K. N. Kudin, J. C. Burant, J. M. Millam, S. S. Iyengar, J. Tomasi, V. Barone, B. Mennucci, M. Cossi, G. Scalmani, N. Rega, , G. A. Petersson, H. Nakatsuji, M. Hada, M. Ehara, K. Toyota, R. Fukuda, J. Hasegawa, M. Ishida, T. Nakajima, Y. Honda, O. Kitao, H. Nakai, M. Klene, X. Li, J. E. Knox, H. P. Hratchian, J. B. Cross, V. Bakken, C. Adamo, J. Jaramillo, R. Gomperts, R. E. Stratmann, O. Yazyev, A. J. Austin, R. Cammi, C. Pomelli, J. W. Ochterski, P. Y. Ayala, K. Morokuma, G. A. Voth, P. Salvador, J. J. Dannen-berg, V. G. Zakrzewski, S. Dapprich, A. D. Daniels, M. C. Strain, O. Farkas, D. K. Malick, A. D. Rabuck, K. Raghavachari, J. B. Foresman, J. V. Ortiz, Q. Cui, A. G. Baboul, S. Clifford, J. Cioslowski, B. B. Stefanov, G. Liu, A. Liashenko, P. Piskorz, I. Komaromi, R. L. Martin, D. J. Fox, T. Keith, M. A. Al-Laham, C. Y. Peng, A. Nanayakkara, M. Challacombe, P. M. W. Gill, B. Johnson, W. Chen, M. W. Wong, C. Gonzalez, J. A.,Pople, Gaussian 03 Revision B.04, Gaussian Inc., Wallingford, *CT*, **2004**.
(35) C. A. Goss, H. D. Abruna, *Inorg. Chem*., 1985, **24**, 4263.
(36) E. C. Glazer, D. Magde, Y. Tor, *J. Am. Chem. Soc.* 2005**, 127**, 4190.
(37) L. Wallace, D. P. Rillema, *Inorg. Chem*., 1993, **32**, 3836.
(38) L. Wallace, C. Woods, D. P. Rillema, *Inorg. Chem*. 1995, **34**, 2875.
(39) L. Wallace, D. C. Jackman, D. P. Rillema, J. W. Merkert, *Inorg. Chem*., 1995, **34**, 5210.
(40) V. Balzani, A. Juris and M. Venturi, *Chem. Rev*., 1996, **96**, 759.
(41) (a) Y. Pellegrin, A. Quaranta, P. Dorlet,M.-F. Charlot,W. Leibl, A. Aukauloo*, Chem.–Eur. J.*, 2005, **11**, 3698; (b) J. D. Lewis, L. Bussotti, P. Foggi, R. N. Perutz, J. N. Moore, *J. Phys. Chem. A*, 2002, **106**, 12202. (c) Y. Wang, K. S. Schanze, *Chem. Phys.*, 1993, **176**, 305.
(42) S. Verma, P. Kar, A. Das, H. N. Ghosh, *Dalton Trans.*, 2011, **40**, 9765.
(43) (a)M.-F.Charlot, Y. Pellegrin, A. Quaranta, W. Leibl, A. Aukauloo, *Chem.–Eur. J.*, 2006, **12**, 796; (b) Y. Pellegrin, A. Quaranta, P. Dorlet, M. F. Charlot, W. Leibl, A. Aukauloo, *Chem.–Eur. J.*, 2005, **11**, 3698
(44) E. C. Glazer, D. Magde, Y. Tor, *J. Am. Chem. Soc*., 2007, **129**, 8544.
(45) K. Nakamato, Application in Coordination, Organometallic and Bioinorganic, John Wiley & Sons, New York, NY, USA, 1997.
(46) K. D. Armond, K. Hanck, G. Kew, *J. Phys. Chem*., 1975, **79**, 1828.
(47) M. Ibrahim, A. Konkin, H. K. Roth, D. Egbe, E. Klemm, U. Zhokhavets, G. Gobsch, S. Sensfuss, *Thin Solid Films*, 2005, **474**, 201.
(48) M. P. Balanay, C. V. P. Dipaling, S. H. Lee, D. H. Kim, K. H. Lee, *Sol. Energ. Mater. Sol. Cel.* 2007, **91**, 1775.
(49) H. Mizuseki, K. Niimura, C. Majumder, R. V. Belosludov, A. A. Farajian, Y. Kwazoe, *Mol. Cryst. Liq. Cryst*. 2003, **406**, 205.
(50) W. M. Campbell, A. K. Burrell, D. L. Officer, K. W. Jolley, *Coord. Chem. Rev*., 2004, **248**, 1363.
(51) H. Mizuseki, N. Igarashi, C. Majumder, A. A. Farajian, J.-T. Wang, H. Chun, Y. Kawazoe, *Mater. Res. Proc*. 2002, **725**, 14.

Dalton Transactions Accepted Manuscript

This journal is © The Royal Society of Chemistry [year]

(52) J. P. Sauvage, J. P. Collin, J. C. Chambron, S. Guillerez, Coudret, C. V. Balzani, F. Barigelletti, L. De Cola, L. Flamigni, *Chem. Rev.,* 1994, **94**, 993.
(53) K. Hara, H. Sugihara, Y. Tachibana, A. Islam, M. Yanagida, K. Sayama. *Langmuir*, 2001, **17**, 5992.
(54) K. Hara, H. Horiuchi, R. Katoh, L. P. Singh, H. Sugihara, K. Sayama, *J. Phys. Chem. B,* 2002, **106**, 374.
(55) C. Yang, H. Chen, Y. Chuang, C. Wu, C. Chen, S. Liao, *J. Power Sources,* **2009**, 188, 627.
(56) S. Huixia, L. Yanhong, G. Xiaozhi, H. Xiaoming, Z. Xiaowei, J. Kejian, M. Qingbo, *Dye. Pig.*, **2010,** 87, 249.
(57) M. K. Nazeeruddin, P. Péchy, T. Renouard, S. Zakeeruddin, M., R. Humphry-Baker, P. Comte, P. Liska, L. Cevey, E. Costa, V. Shklover, L. Spiccia, G. B. Deacon, C. A. Bignozzi, M. Gratzel, *J. Am. Chem. Soc.,* **2001**, 123, 1613.
(58) G. P. Bomben, K. C. D. Robson, B. D. Koivisto, C. P. Berlinguette, *Coord. Chem. Rev*. **2012**, 256, 1438.
(59) F. Angelis, D. Fantacci, S. Selloni, M. Gratzel,; Md, M.; Nazeeruddin, *Nano Lett*., 2007, **7**, 3189.
(60) O. Schwarz, D. V. Loyen, S. Jockusch, J. Turro, N. Heinz Dürr, *J. Photochem. Photobiol. A: Chem.,* 2000, **132**, 91.
(61) C. Alleyne,. S. K. O. Mailer, *Can. J. Chem*., 1974, **52**, 336.
(62) A. L. Arduini, M. Garnett, R. C. Thompson, T. C. T. Wong, *Can. J. Chem*., 1975, **53**, 3812.
(63) J. H. Lora, M. Wayman, *Can. J. Chem*., **1980**, 58, 669.
(64) M. Xu, R. Li, N. Pootrakulchote, D. Shi, J. Guo, Z. Yi, *J. Phys. Chem. C,* **2008**, 112, 19770.

Dalton Transactions Accepted Manuscript

Graphical abstract

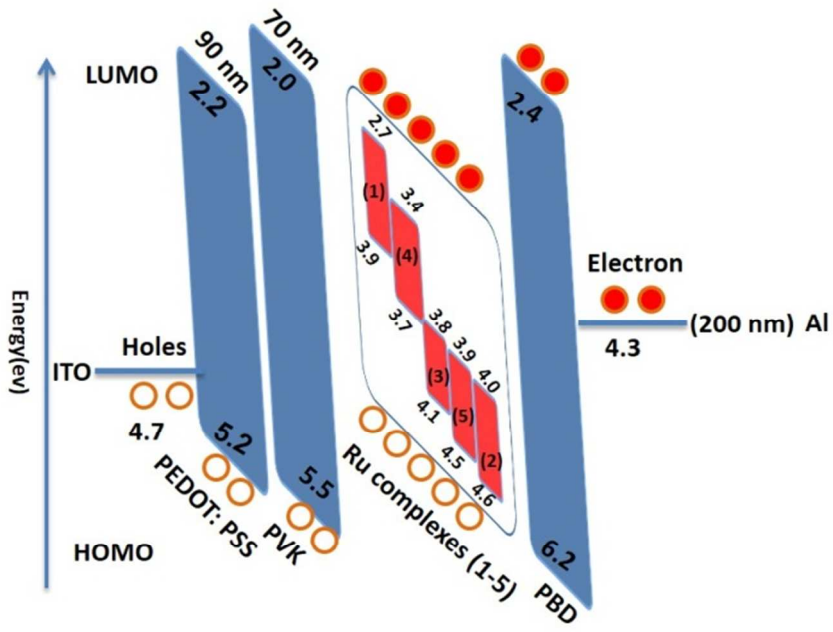

Dalton Transactions Accepted Manuscript